Anisotropy signature in RTM extended images

Paul Sava[1] & Tariq Alkhalifah[2]
[1]*Center for Wave Phenomena, Colorado School of Mines*
[2]*King Abdullah University of Science and Technology*

ABSTRACT
Reverse-time migration can accurately image complex geologic structures in anisotropic media. Extended images at selected locations in the earth, i.e. at common-image-point gathers (CIPs), carry rich information to characterize the angle-dependent illumination and to provide measurements for migration velocity analysis. However, characterizing the anisotropy influence on such extended images is a challenge. Extended CIPs are cheap to evaluate, since they sample the image at sparse locations indicated by the presence of strong reflectors. Such gathers are also sensitive to velocity error which manifests itself through moveout as a function of space and time lags. Furthermore, inaccurate anisotropy leaves a distinctive signature in CIPs, which can be used to evaluate anisotropy through techniques similar to the ones used in conventional wavefield tomography. It, specifically, admits a "V"-shape residual moveout with the slope of the "V" flanks depending on the ellipticity anisotropic parameter η regardless of the complexity of the velocity model. It reflects the fourth-order nature of the anisotropy influence on moveout, as it manifests it self in this distinct signature in extended images after handling the velocity properly in the imaging process. Synthetic and real data observations support this assertion.

Key words: imaging, wave-equation, angle-domain, wide-azimuth, anisotropy

1 INTRODUCTION

Wave-equation depth migration is powerful and accurate for imaging complex geology, but its potential can only be achieved with high quality models of the earth (Gray et al., 2001). Imaging using reverse-time migration (Baysal et al., 1983; McMechan, 1983), addresses this challenge, although this technique is still fairly computationally intensive, especially in anisotropic media.

Imaging with reverse-time migration can be described as a sequence of two main steps. The first step consists of wavefield reconstruction from known quantities on the surface, i.e. the wavelet known at the source position, and the data known at the receiver positions. The wavefields are reconstructed everywhere in the medium as a solution of the wave-equation. This reconstruction makes use of an earth model which can be, for example, anisotropic. The second step represents an imaging condition, i.e. a procedure that identifies places in the subsurface where the reconstructed wavefields coincide. The imaging condition is often implemented by cross-correlation of the wavefields. A general imaging condition preserves in the output the space and time correlation lags, and thus it can be named an extended imaging condition for which the conventional cross-correlation is a special case.

Assuming that the wavefields are accurately reconstructed in the subsurface, the correlation maximizes at zero lag, both in space and in time. Accurate reconstruction implies not only that we use a correct earth model, but it also implies that the recorded data illuminates completely the subsurface in the area under investigation. Good illumination requires not only that we collect data with wide azimuth and long offsets, but it also means that the geologic structure does not obstruct our imaging target inside the earth through, for example, shadows caused by salt bodies.

Typically, the problem of large output can be addressed by analyzing subsets of the image. For example, we can consider common-image-gathers (CIGs), which are subsets of extended images constructed for various lags at fixed horizontal coordinates in the earth. For example, we can consider space-lag CIGs (Rickett and Sava, 2002) , or time-lag CIGs (Sava and Fomel, 2006) , which can be transformed into angle-gathers (Sava and Fomel, 2003) for easier analysis for even anisotropic media (Sava and Alkhalifah, 2012; Alkhalifah and Fomel, 2011). Alternatively, we can construct common-image-point-gathers (CIPs), which are subsets of extended images constructed for all lags at fixed coordinates in the image. The points where we construct the gathers can be identified automatically using image features, e.g. reflectivity strength, spatial coherency, etc. (Cullison and Sava, 2011) .

In anisotropic media, the extrapolation of the source and

receiver fields need to take anisotropy into account. This requires that we have access to proper anisotropic parameter description of the medium. For transversely isotropic (TI) media, this implies that we need to know the anisotropy model parameter, η, responsible for the anellipticity behavior of the phase velocity. This parameter, together with the normal moveout velocity described along the symmetry axis direction, enables us to perform accurate imaging in TI media (Alkhalifah et al., 2001). The axis of symmetry velocity, v_{p_z}, for a medium with vertical symmetry axis is mainly responsible for placing reflections at their accurate depth positions. Thus, for anisotropic media the key parameter for proper imaging and focussing is η. Ignoring η yields residual moveout in subsurface offsets and angle gathers (Alkhalifah and Fomel, 2011); it yields even more distinct features in extended images.

In this paper, we analyze the extended images in anisotropic media, and specifically transversely isotropic (TI) media. These extended images provide image point extensions as a function of space- and time-lags. Embedded in these lag sections is valuable image focusing information, which can be used to analyze the model accuracy used in the wavefield extrapolation. As a result, we use such lag sections to characterize the response of the extended images to ignoring anisotropy in RTM. We find that the anisotropy error leaves a distinctive signature in migrated extended images. We restrict our attention to the analysis of migrated images, and explore in detail the specific information provided by such images for anisotropic wavefield tomography.

2 THEORY

Conventional wavefield-based imaging consists of two major steps: the wavefield reconstruction and the imaging condition (Berkhout, 1982; Clærbout, 1985). The major driver for the accuracy of this technique are the source and receiver wavefields which depend on space $\mathbf{x} = \{x, y, z\}$ and time t. Wavefield reconstruction in tilted TI anisotropic medium, requires numeric solutions to a pseudo-acoustic wave-equation (Alkhalifah, 2000), e.g. the time-domain method of Fletcher et al. (2009) and Fowler et al. (2010), which consists of solving a system of second-order coupled equations:

$$\frac{\partial^2 p}{\partial t^2} = v_{p_x}^2 H_2\left[p\right] + v_{p_z}^2 H_1\left[q\right] \ , \tag{1}$$

$$\frac{\partial^2 q}{\partial t^2} = v_{p_n}^2 H_2\left[p\right] + v_{p_z}^2 H_1\left[q\right] \ . \tag{2}$$

Here, p and q are two wavefields depending on space $\mathbf{x}$ and time t, H_1 and H_2 are differential operators applied to the quantity in the square brackets Alternative formulations, e.g. Duveneck and Bakker (2011) and Zhang et al. (2011) provide expressions for stable extrapolation in more general cases, including TTI. The velocities v_{p_z}, v_{p_x}, and v_{p_n} are the vertical, horizontal and "NMO" velocities used to parametrize a generic TTI medium. If we describe the medium using the parameters introduced by Thomsen (2001), the velocities are related to the anisotropy parameters ϵ and δ by the relations $v_{p_n} = v_{p_z}\sqrt{1+2\delta}$ and $v_{p_x} = v_{p_z}\sqrt{1+2\epsilon}$. Thus, the quantities H_1 and H_2 depend on the medium parameters, as well as θ_a which describes the angle made by the TI symmetry axis with the vertical and ϕ_a the azimuth angle of the plane that contains the tilt.

A conventional imaging condition based on the reconstructed wavefields defines the image as the zero lag of the cross-correlation between the source and receiver wavefields (Clærbout, 1985). An extended imaging condition is a generalization of the conventional imaging condition in that it retains in the output image acquisition or illumination parameters. For example, we can generate image extensions by correlation of the wavefields shifted symmetrically in space (Rickett and Sava, 2002; Sava and Fomel, 2005) or in time (Sava and Fomel, 2006). This separation is simply the lag of the cross-correlation between the source and receiver wavefields (Sava and Vasconcelos, 2011):

$$R\left(\mathbf{x}, \boldsymbol{\lambda}, \tau\right) = \sum_{shots} \sum_{t} W_s\left(\mathbf{x} - \boldsymbol{\lambda}, t - \tau\right) W_r\left(\mathbf{x} + \boldsymbol{\lambda}, t + \tau\right) \ . \tag{3}$$

Here R represents the migrated image which depends on position $\mathbf{x}$, and the quantities $\boldsymbol{\lambda}$ and τ are cross-correlation lags in space and time, respectively. The source and receiver wavefields used for imaging, W_s and W_r are the main wavefields indicated by p in equations 1-2. The conventional imaging condition represents a special case of equation 3 for $\boldsymbol{\lambda} = 0$ and $\tau = 0$.

Various techniques have been proposed to convert the space- and time-lag extensions into reflection angles (Sava and Fomel, 2003, 2006; Sava and Vlad, 2011; Sava and Alkhalifah, 2012), thus facilitating amplitude and velocity analysis in complex geologic structures. In this paper, we do not follow this route, but instead concentrate on the interpretation of the moveout observed as a function of lags directly. A similar analysis can be done in the angle domain, but in this paper we disregard this possibility.

As indicated earlier, CIPs constructed using a correct earth model (and good subsurface illumination) reveal reflections as focused events at zero space- and time-lags. This shape has a straightforward physical interpretation. Following the discussion in Sava and Vlad (2011), the wavefield at a reflection point can be conceptually decomposed in planar components, each corresponding to a different propagation direction. We emphasize that we use the word "decomposition" only with a conceptual meaning, and not a practical one. Other researchers have proposed actual decomposition of the wavefields in elementary planar components with different directions, but we do not follow that path which is costlier and more difficult to implement in practice.

Nevertheless, the source and receiver wavefields at a reflection point where we construct a CIP gather behave as if they were strictly planar. Other planar components of the same non-planar wavefield exist, but they are located elsewhere in space, and thus do not contribute to the CIP under consideration. By simultaneously shifting the source and receiver wavefields in space and time, we obtain non-zero images only when the space- and time-lags are related to one-another by a rela-

tion which depends on the 3D angles of incidence and local material properties, (Sava and Vlad, 2011). It turns out that each direction of illumination is described in a CIP by a planar event in the $\boldsymbol{\lambda} - \tau$ space. This observation is true both for isotropic and anisotropic media, but the physical interpretation is different: in isotropic media, the planar events identify directions corresponding to group angles, while in anisotropic media the planar events identify directions corresponding to phase angles, (Sava and Alkhalifah, 2012).

The most relevant property for velocity model building is that the planar events corresponding to different illumination directions overlap at zero space and time lag, i.e. at the origin of the extended space of each CIP. This is simply because we choose, by construction, points on reflectors, so ideally we form an image at zero lag from all propagation directions at the same place on the reflector. This is just a restatement of the semblance principle which says that the imaged geologic structure does not depend on the direction of illumination, assuming that the model used for wavefield reconstruction is correct. If the reconstruction is incorrect, then not all planar events in a CIP go through zero lag in space and time, thus indicating that not all illumination directions produce the image at the same depth. This information can be used for velocity analysis.

In anisotropic media, wavefield reconstruction depends on more than one parameter. For TI media, one simple way to describe the model parameters is through velocity v and the anisotropic parameter η. Reconstructed wavefields can be inaccurate due to inaccuracies in both parameters, so the effects observed in extended CIPs are simultaneously due to both. As for other domains, it is not trivial to differentiate between the effects of velocity and anisotropy error on the model. It is, nevertheless, interesting to understand how each parameter controls the observed moveout, which is a pre-requisite for tomography. Thus, we concentrate on the moveout due to anisotropy, assuming that the velocity has already been updated using other conventional methods. This is natural since the common velocity model building procedure starts with an isotropic assumption of the Earth.

Alkhalifah and Fomel (2011) show using anisotropic parameter continuation that the residual anisotropic response for post stack imaging in homogeneous media, and specifically residuals corresponding to the anisotropy parameter η, has a "V"-like shape. This response stems from the fourth-order nature of the η influence on travel-time as a function of offset. A residual reconstruction of such travel-time maps the fourth order influence to a mostly linear moveout, rather than a residual hyperbolic moveout, as shown in Figure 1. The slope of the V depends on the value of η, with negative η reverting its signature. A similar response characterizes the prestack case even in complex media.

The V-shape signature in the extended images exists regardless of the complexity of the background isotropic (or elliptically anisotropic) velocity model. Thus, such a behavior also characterizes the extended images for pre-stack data in complex anisotropic media. This is because the major wavefield complexities are compensated during the wavefield reconstruction in anisotropic media. Most of what remains are the influence of anisotropy which resembles the established behavior of poststack depth images. This property could be used to separate the effects of anisotropy from those of velocity, with applications to anisotropic earth model building.

3 EXAMPLES

The model for our first example, Figure 2(c), consists of a horizontal reflector in a 3D constant velocity model. Figures 2(a)-2(b) depict one snapshot of the wavefields for a source located on the surface in VTI and TTI models, respectively. The models are characterized by the parameters $\epsilon = 0.30$, $\delta = -0.10$ and, for the TTI model, by $\theta_a = 35^\circ$ and $\phi_a = 45^\circ$. Figures 3(a)-3(b) depict extended CIPs at $\{x, y, z\} = \{4, 4, 1\}$ km for many sources distributed uniformly on the surface and correct earth models. All CIPs show focusing at zero lags in space and time, thus indicating wavefield reconstruction with a correct earth model. However, the CIPs constructed with isotropic migration, Figures 3(c) and 3(d), are not focused, thus indicating that the CIPs are sensitive to anisotropy inaccuracy.

The next examples illustrate the behavior of the extended images as a function of anisotropy inaccuracy in constant and laterally heterogeneous models, respectively. The models are shown in Figures 4(a) and 6(a). The data, exemplified in Figures 4(b) and 6(b), are constructed with anisotropy characterized by parameter $\eta = 0.25$. Figures 7(a)-7(c) show the extended images for different shot locations obtained by reverse-time migration with the correct salt model. The figures indicate a dependency of the CIPs with the angle of illumination which can be exploited for angle decomposition. The summation for all shots leads to the CIP shown in Figure 7(e) which shows focusing of the image at zero space and time lags. This is due to the fact that all shots leave an imprint on the CIPs at zero space and time lags, but at different slopes which depend on the illumination angle, Figures 7(a)-7(c).

For incorrect η, the resulting response has an overall "V" shape similar to that seen for residual poststack migration. The slope of the "V" flanks, as illustrated in Figures 7(d)-7(f), depend on η. For η close to the correct value, the "V" energy tends to approach the apex, and for correct η it focuses at its apex, Figure 7(e). This general behavior is consistent regardless of the complexity of the medium, especially with respect to the portion of the signature that is near the apex. For comparison, Figures 5(d)-5(e) show extended gathers corresponding to the same values of η as in Figures 7(d)-7(e). Despite the fact that the background velocity model is significantly different, constant vs. salt, the CIPs are comparable, thus indicating that they are mainly influenced by the anisotropy parameters. Of course, for a varying η, such signatures reflect an effective value under the effective medium theory. This property can be exploited for anisotropic migration velocity analysis.

FInally, Figures 8(a)-8(b) illustrate the behavior of 3D anisotropic extended CIPs for a North Sea field dataset. Figure 8(a) shows the velocity model and Figure 8(b) shows the corresponding conventional image. Although the earth is

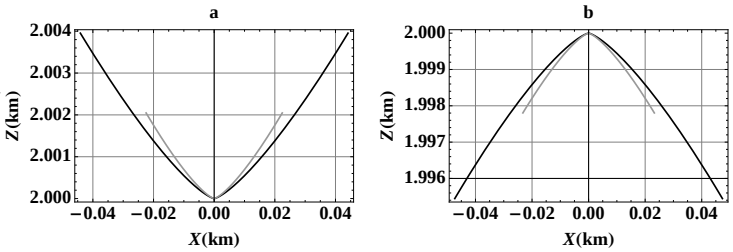


Figure 1. Image point defocusing corresponding to isotropic poststack migration with the correct velocity of 2 km/s in an anisotropic medium with (a) $\eta = 0.1$ (grey curve), $\eta = 0.2$ (black curve), (b) $\eta = -0.1$ (grey curve), and $\eta = -0.2$ (black curve).

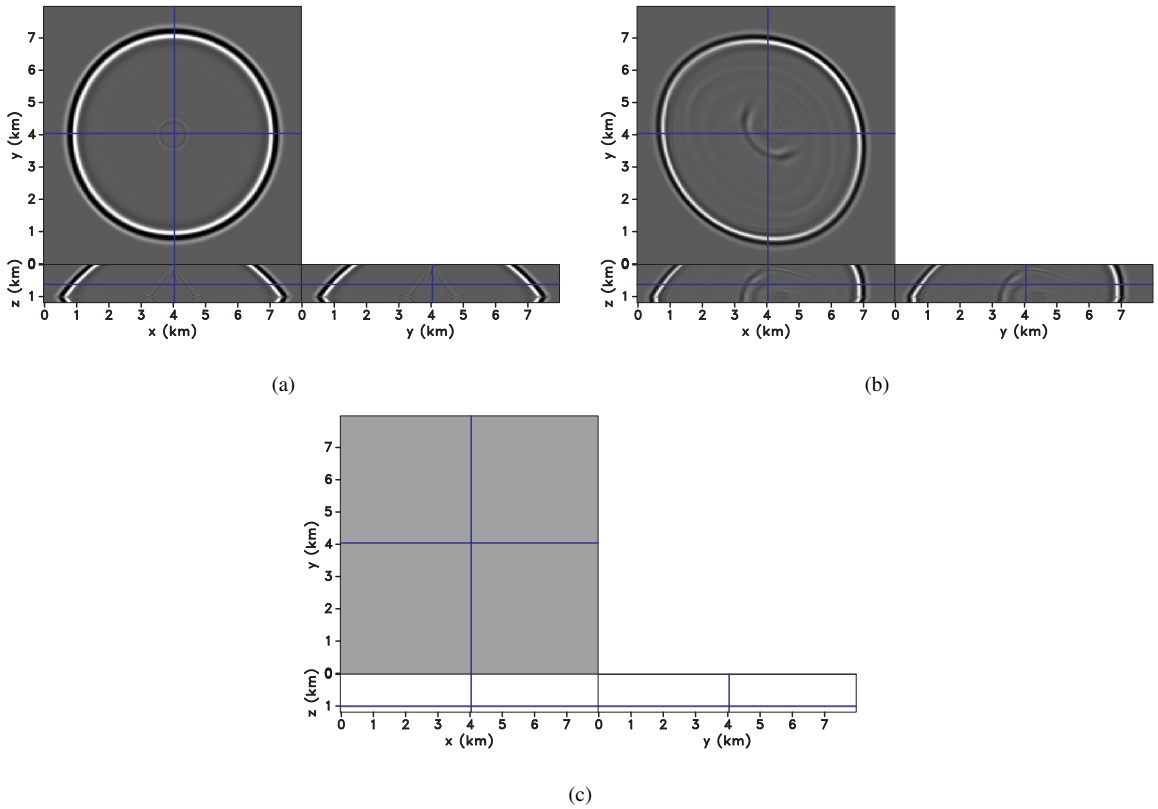


Figure 2. 3D model used to illustrate wide-azimuth extended images in anisotropic media. Panels (a) and (b) show the wavefields corresponding to a single source at $\{x, y\} = \{4, 4\}$ km for VTI and TTI media, respectively. The model (c) consists of a horizontal reflector in constant velocity.

known to be anisotropic in this region, the image shown in Figure 8(b) uses isotropic migration, and thus it is partially inaccurate.

Figure 9 shows the same image as the one shown in Figure 8(b), but in a perspective view and with three slices selected at a fixe inline, cross-line and depth, respectively. Overlain on the figure are also the locations of the CIPs constructed to analyze the accuracy of the image. CIPs are indicated by small ellipsoids instead of points, (Cullison and Sava, 2011). The flat ellipsoids represent the structure tensor constructed at each point, and the orientation of the ellipsoids in 3D space indicates the orientation of the reflectors at each position. We construct extended CIPs at each of these 5000 locations, which represents an enormous cost reduction relative to CIGs constructed for all depths at many regularly-spaced positions on the surface.

Figures 10(a)-10(b) depict different locations in the image, corresponding to CIPs automatically using the method discussed earlier.

In Figure 10(b), the CIP is selected in the middle of the image, therefore the inline illumination is good, although the cross-line aperture is more limited. In the inline direction, we observe the characteristic V, indicating that the model currently used for imaging is actually accurate, but the anisotropy is not accurate. The inline behavior should, in principle, repeat in the cross-line direction, although this is not what happens in this case due to the limited aperture. Partial illumination is also visible in Figure 10(b). In this case, we see a CIP located at the

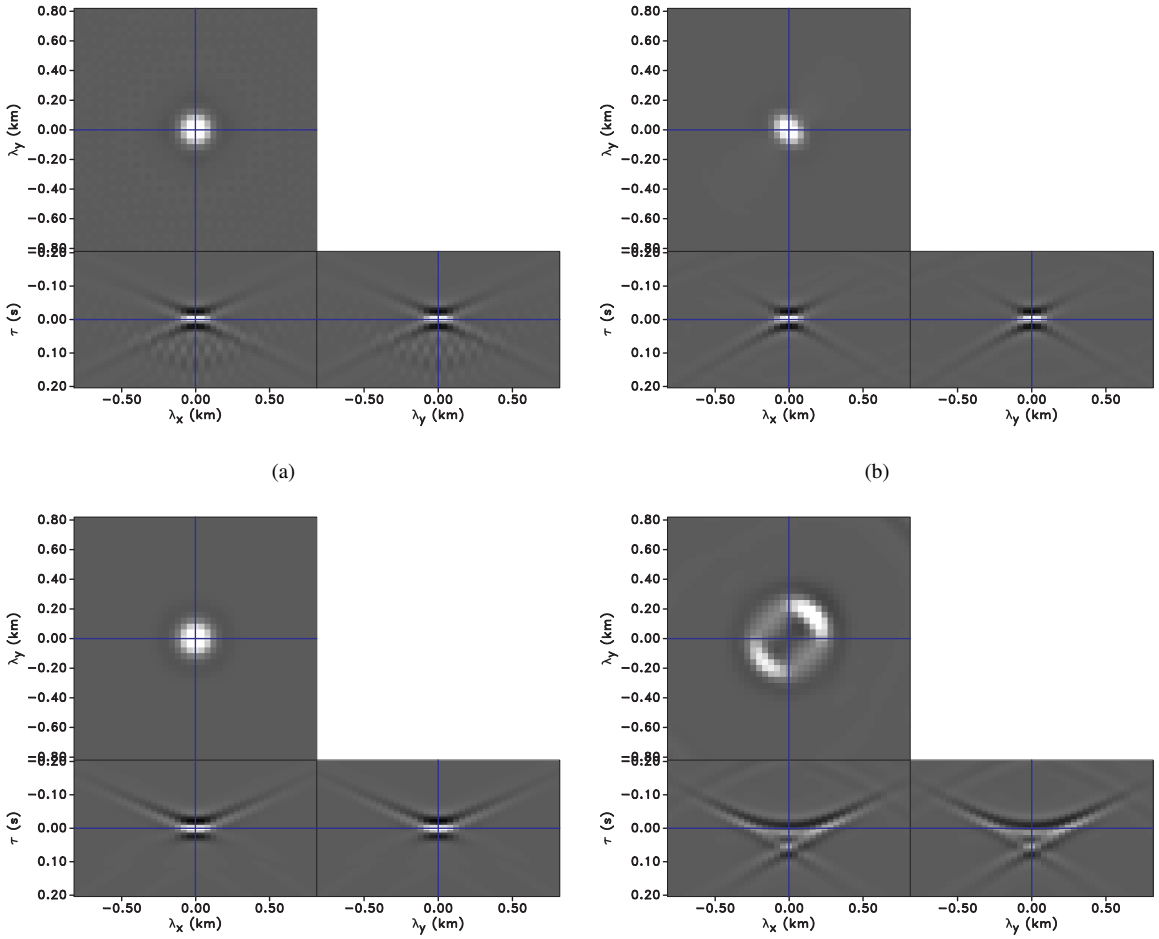


Figure 3. Extended CIPs at $\{x, y, z\} = \{4, 4, 1\}$ km for many sources distributed uniformly on the surface. The images are obtained by (a)-(b) isotropic migration, and (c)-(d) anisotropic migration of the VTI data (left) and TTI data (right).

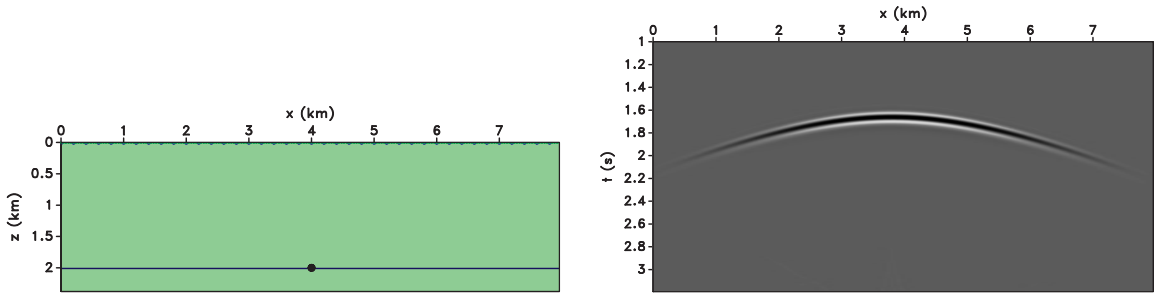


Figure 4. (a) 2D **constant model** used to study the dependence of the extended CIPs with anisotropy, and (b) one shot gather for a source located at $\{x, z\} = \{3.4, 0\}$ km. The earth model is anisotropic and characterized by parameter $\eta = 0.25$.

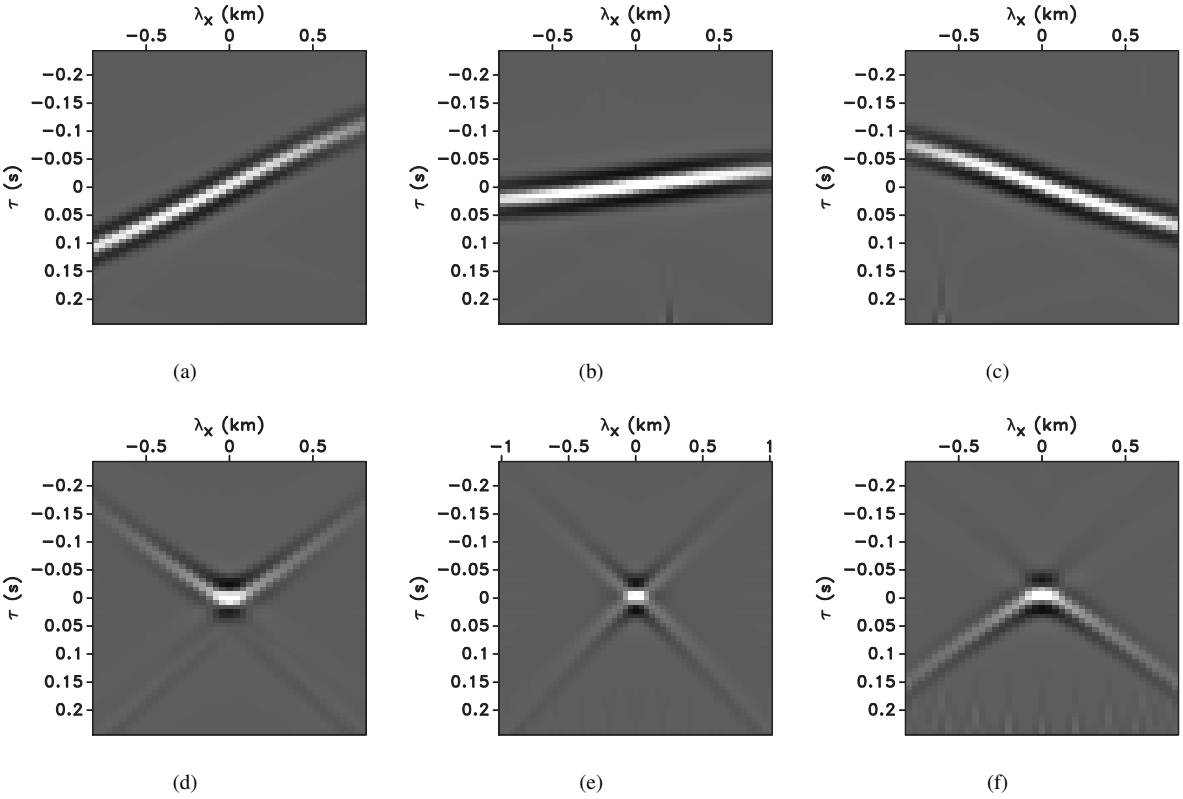


Figure 5. 2D extended CIPs at $\{x, z\} = \{4, 0\}$ km for the **constant model**, Figure 6(a). The extended images (a)-(c) correspond to individual shots at surface coordinates $x = \{3.2, 4.0, 4.8\}$ km and are obtained from wavefields reconstructed with the correct $\eta = 0.25$. The extended images (d)-(f) correspond to anisotropy characterized by parameter $\eta = \{0.15, 0.25, 0.35\}$.

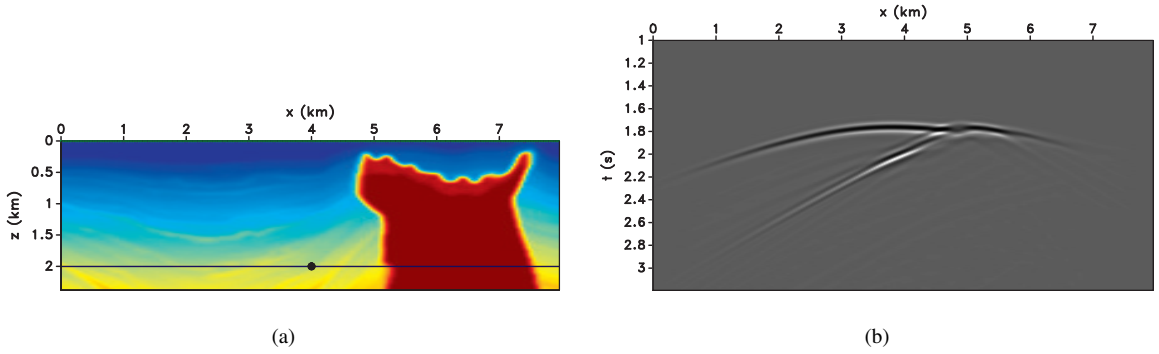


Figure 6. (a) 2D **salt model** used to study the dependence of the extended CIPs with anisotropy, and (b) one shot gather for a source located at $\{x, z\} = \{3.4, 0\}$ km. The earth model is anisotropic and characterized by parameter $\eta = 0.25$.

edge of the model, where the illumination is mainly from one side even in the inline direction.

4 CONCLUSIONS

The distinct anisotropic signatures, needed for parameter estimation, tend to get lost in the mist of the complexity of the velocity in the medium. Extended images preserve such signatures, which allows for direct anisotropy analysis. The slope of the residual moveout in extended CIPs mainly depends on η, which simplifies parameter estimation in anisotropic media. A comparison of extended images between simple and complex models supports our assertion.

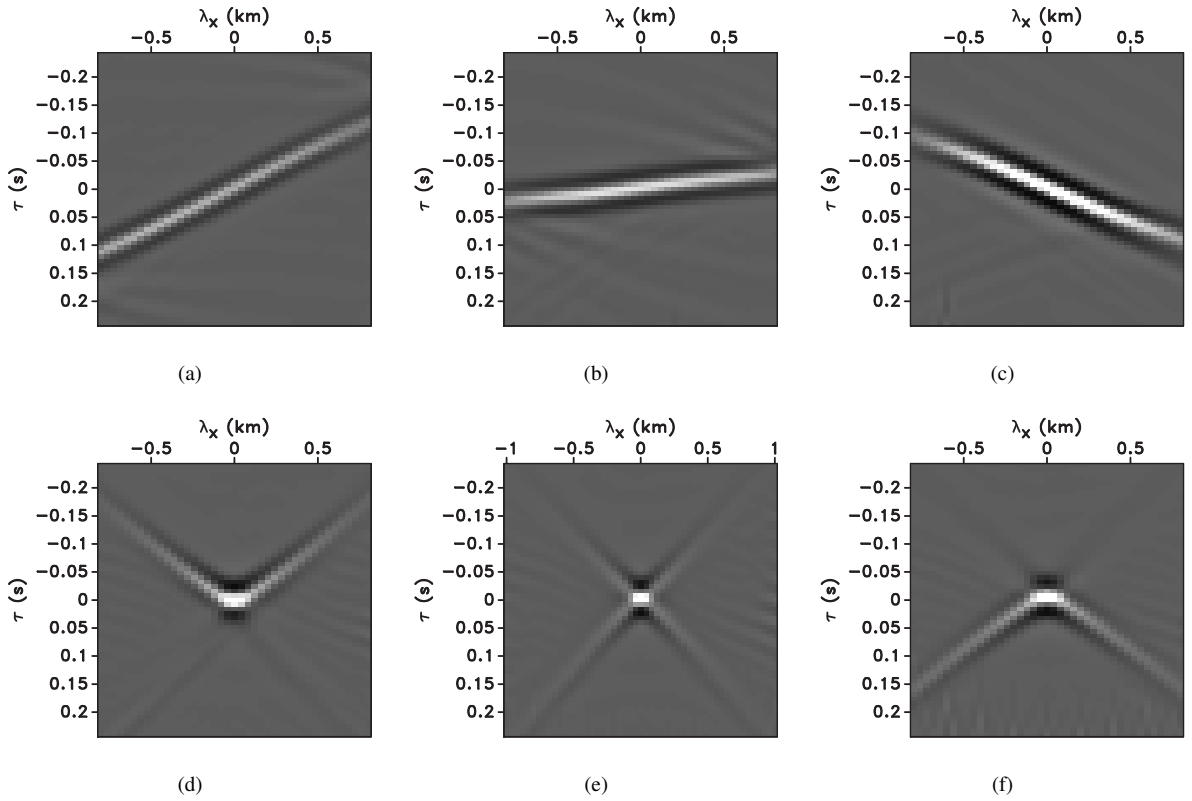


Figure 7. 2D extended CIPs at $\{x, z\} = \{4, 0\}$ km for the **salt model**, Figure 6(a). The extended images (a)-(c) correspond to individual shots at surface coordinates $x = \{3.2, 4.0, 4.8\}$ km and are obtained from wavefields reconstructed with the correct $\eta = 0.25$. The extended images (d)-(f) correspond to anisotropy characterized by parameter $\eta = \{0.15, 0.25, 0.35\}$.

5 ACKNOWLEDGMENTS

The authors would like to thank Statoil ASA and the Volve license partners, ExxonMobil E&P Norway and Bayerngas Norge, for the release of the Volve data. Partial funding for this research is provided by KACST. The reproducible numeric examples in this paper use the Madagascar open-source software package freely available from http://www.ahay.org.

REFERENCES

Alkhalifah, T., 2000, An acoustic wave equation for anisotropic media: Geophysics, **65**, 1239–1250.

Alkhalifah, T., and S. Fomel, 2011, The basic components of residual migration in VTI media using anisotropy continuation: J Petrol Explor Prod Technol, **1**, 17–22.

Alkhalifah, T., S. Fomel, and B. Biondi, 2001, The space-time domain: theory and modelling for anisotropic media: Geophysical Journal International, **144**, 105–113.

Baysal, E., D. D. Kosloff, and J. W. C. Sherwood, 1983, Reverse time migration: Geophysics, **48**, 1514–1524.

Berkhout, A. J., 1982, Imaging of acoustic energy by wave field extrapolation: Elsevier.

Clærbout, J. F., 1985, Imaging the Earth's interior: Blackwell Scientific Publications.

Cullison, T., and P. Sava, 2011, An image-guided method for automatically picking common-image-point gathers: Presented at the 81st Annual International Meeting, SEG, Expanded abstracts.

Duveneck, E., and P. M. Bakker, 2011, Stable P-wave modeling for reverse-time migration in tilted TI media: Geophysics, **76**, S65–S75.

Fletcher, R. P., X. Du, and P. J. Fowler, 2009, Reverse time migration in tilted transversely isotropic (TTI) media: Geophysics, **74**, WCA179–WCA187.

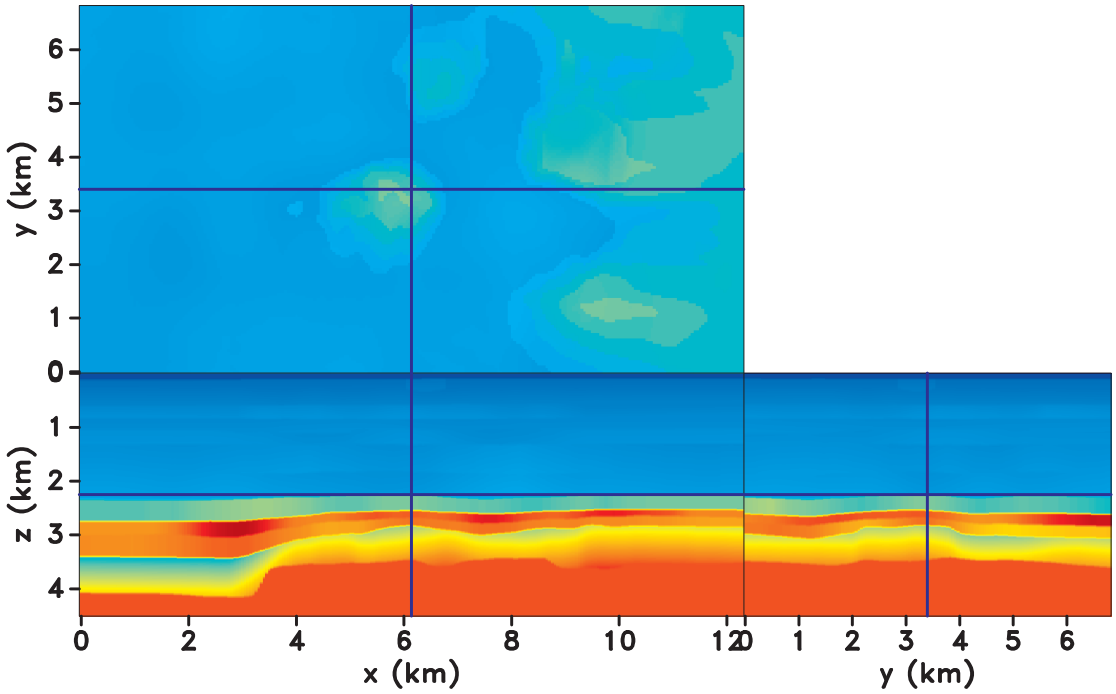
Fowler, P. J., X. Du, and R. P. Fletcher, 2010, Coupled equations for reverse time migration in transversely isotropic media: Geophysics, **75**, S11–S22.

Gray, S. H., J. Etgen, J. Dellinger, and D. Whitmore, 2001, Seismic migration problems and solutions: Geophysics, **66**, 1622–1640.

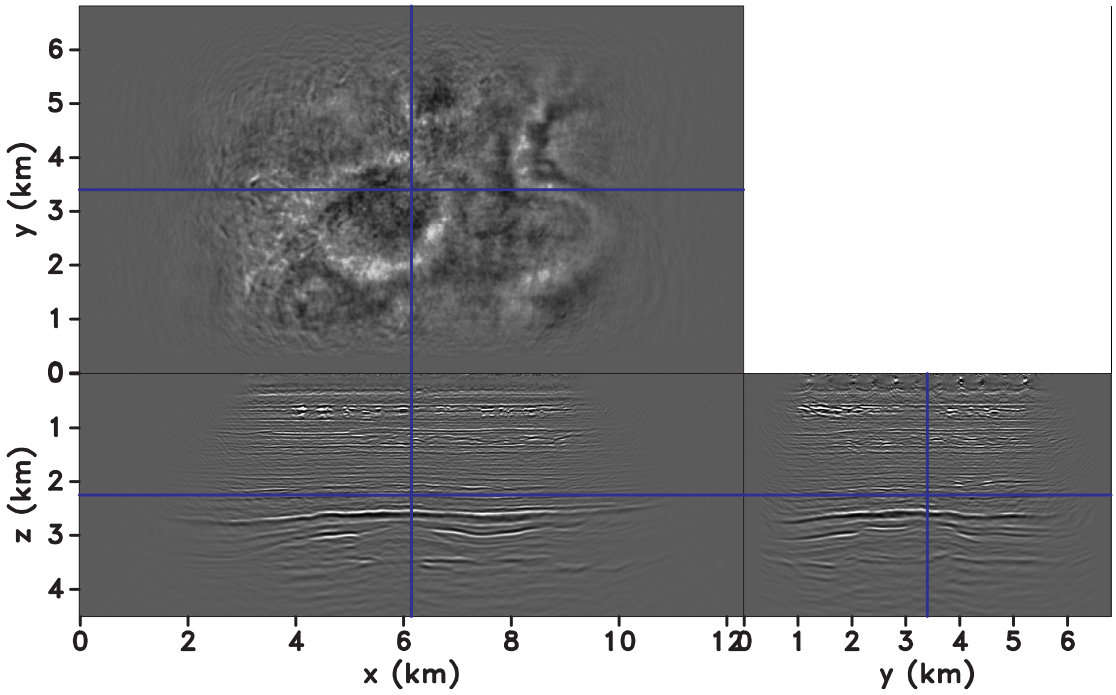
McMechan, G. A., 1983, Migration by extrapolation of time-dependent boundary values: Geophys. Prosp., **31**, 413–420.

Rickett, J., and P. Sava, 2002, Offset and angle-domain common image-point gathers for shot-profile migration: Geophysics, **67**, 883–889.

Sava, P., and T. Alkhalifah, 2012, Wide-azimuth angle gathers for anisotropic wave-equation migration: Geophysical



(a)



(b)

Figure 8. North Sea model: (a) P-wave velocity, and (b) isotropic image.

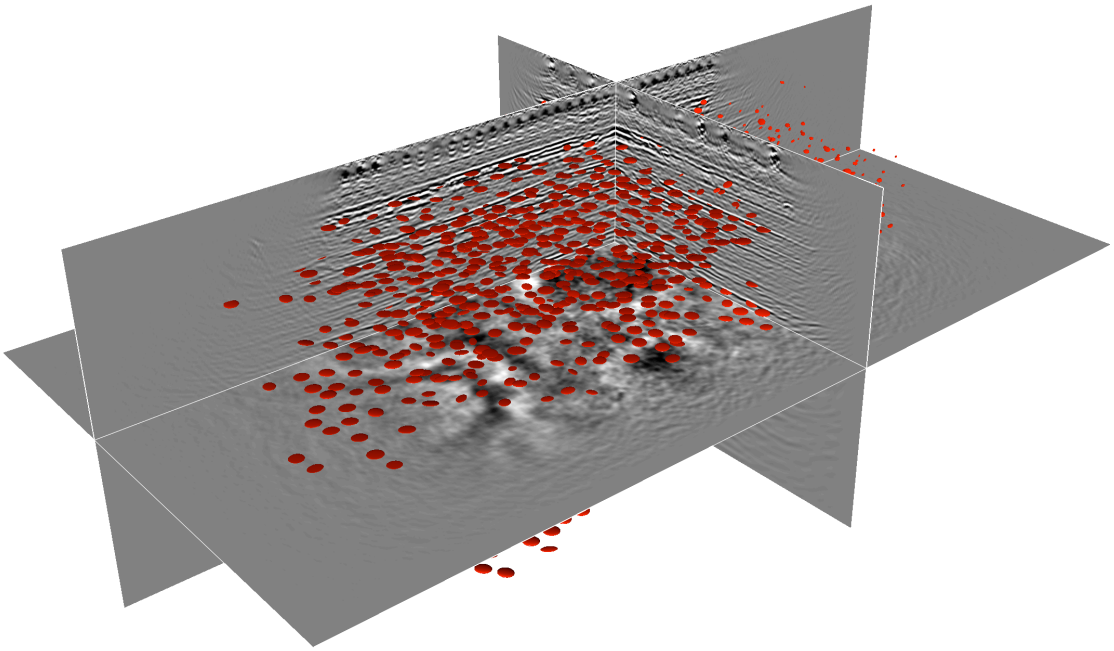


Figure 9. Image with the picked locations of the CIP gathers. The ellipsoids indicate the local slope and azimuth of the geologic structure.

Prospecting, in press.

Sava, P., and S. Fomel, 2003, Angle-domain common image gathers by wavefield continuation methods: Geophysics, **68**, 1065–1074.

———, 2005, Coordinate-independent angle-gathers for wave equation migration: 75th Annual International Meeting, SEG, Expanded Abstracts, 2052–2055.

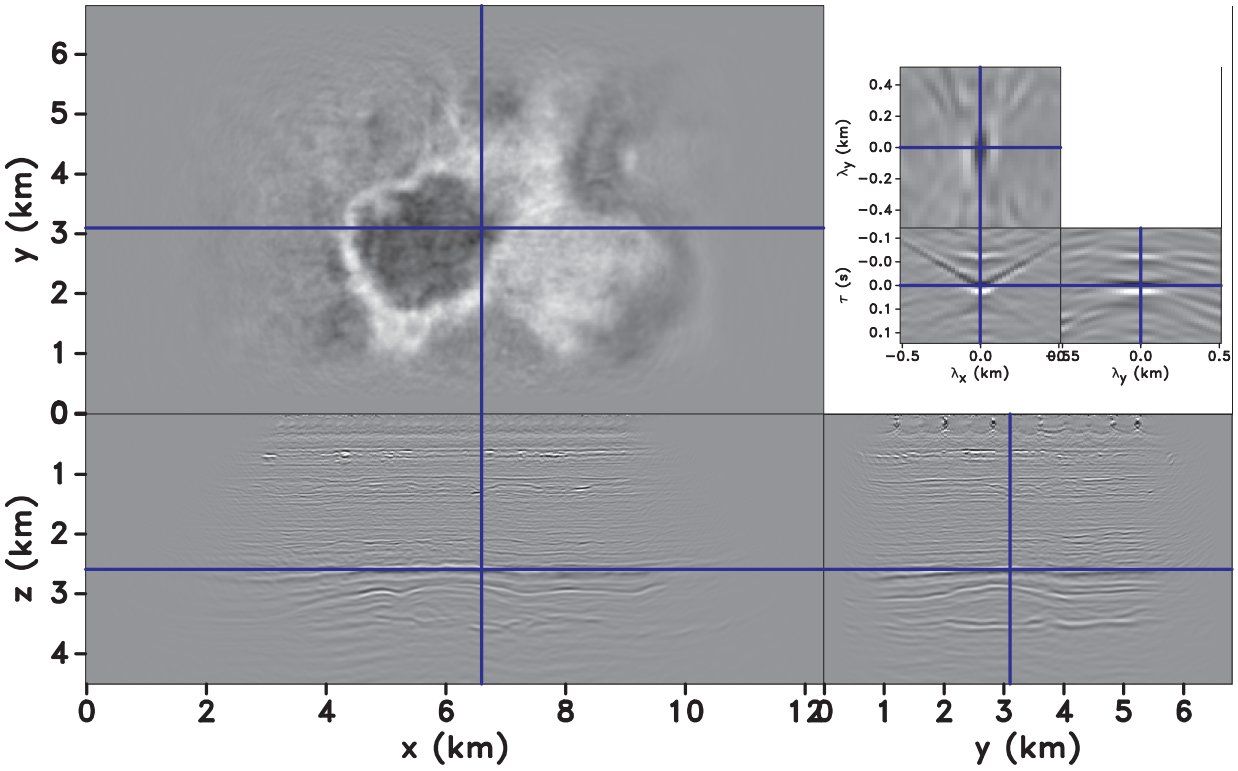
———, 2006, Time-shift imaging condition in seismic migration: Geophysics, **71**, S209–S217.

Sava, P., and I. Vasconcelos, 2011, Extended imaging condition for wave-equation migration: Geophysical Prospecting, **59**, 35–55.

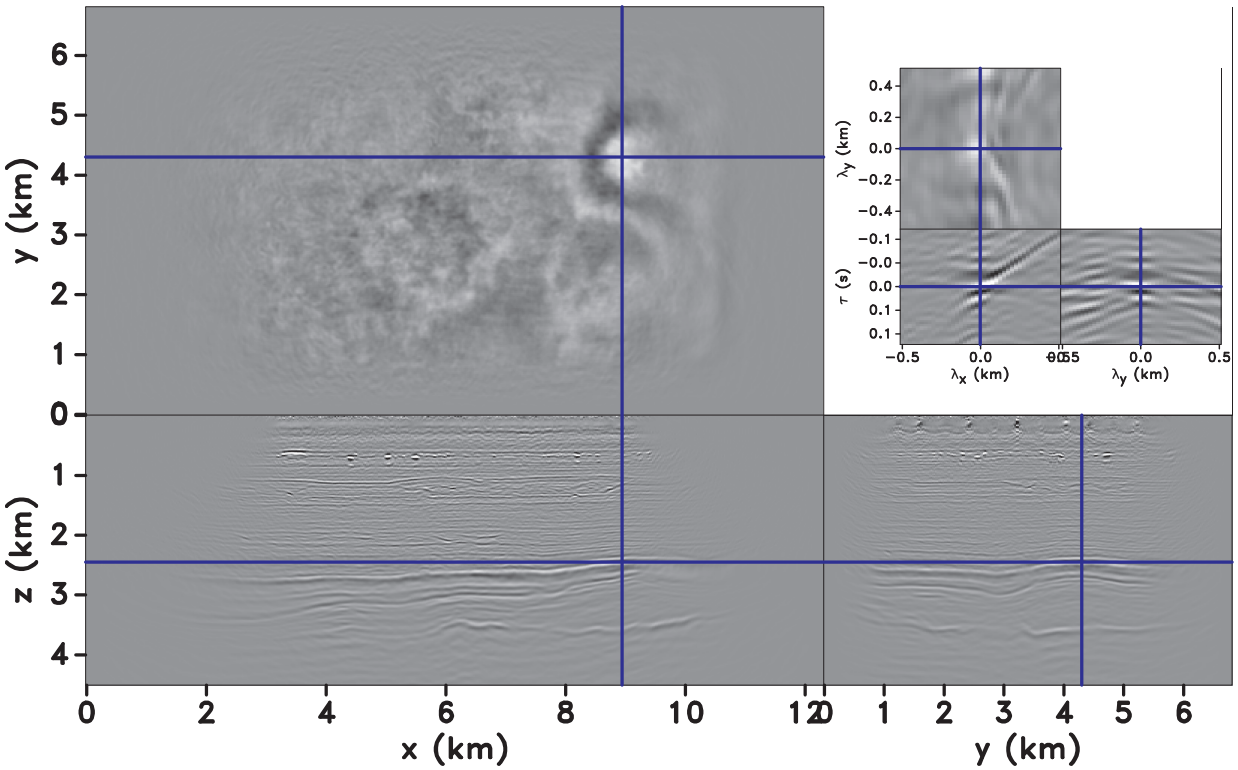
Sava, P., and I. Vlad, 2011, Wide-azimuth angle gathers for wave-equation migration: Geophysics, **76**, S131–S141.

Thomsen, L., 2001, Seismic anisotropy: Geophysics, **66**, 40–41.

Zhang, Y., H. Zhang, and G. Zhang, 2011, A stable TTI reverse time migration and its implementation: Geophysics, **76**, WA3–WA11.



(a)



(b)

Figure 10. Conventional images with inset indicating the extended image at the coordinates marked by the intersecting lines.